



ISSN: 0067-2904

## Texture Features of Grey Level Size Zone Matrix for Breast Cancer Detection

Rasha Awad Abtan<sup>1</sup>, Anwar H. Al-Saleh<sup>2</sup>, Haidar J. Mohamed<sup>3</sup>, Heba Kh. Abbas<sup>4</sup>, Ali A. Alzuky<sup>3</sup>

<sup>1</sup>Department of Computer, Basic education college, Mustansiriyah University, Baghdad, Iraq

<sup>2</sup>Department of Computer Science, College of Science, Mustansiriyah University, Baghdad, Iraq

<sup>3</sup>Department of Physics, College of Science, Mustansiriyah University, Baghdad, Iraq

<sup>4</sup>Department of Physics, College of Science for Women, University of Baghdad, Baghdad, Iraq

Received: 25/6/2022

Accepted: 26/8/2022

Published: 30/1/2023

### Abstract

The texture analysis of cancer cells leads to a procedure to distinguish spatial differences within an image and extract essential information. This study used two test tumours images to determine cancer type, location, and geometric characteristics (area, size, dimensions, radius, etc.). The suggested algorithm was designed to detect and distinguish breast cancer using the segmentation-based threshold technique. The method of texture analysis Grey Level Size Zone method was used to extract 11 features: Small Zone Emphasis, Large Zone Emphasis, Low Grey Level Zone Emphasis, High Grey Level Zone Emphasis, Small Zone Low Grey Level Emphasis, Small Zone High Grey Level Emphasis, Large Zone Low Grey Level Emphasis, Large Zone High Grey Level Emphasis, Grey Level Non-Uniformity Normalized, Grey Level Non-Uniformity, and Zone Percentage. The results show that the tumour's location is highly accurate depending on the extracting properties. The results of the suggested method give the decision to identify the type of tumours. The geometry of the tumour helps describe the tumour.

**Keywords:** Breast Cancer, Size Zone Matrix, Geometric properties, segmentation.

### مميزات نسيج مصفوفة منطقة الحجم مستوى الرمادي لاكتشاف سرطان الثدي

رشا عواد عبطان<sup>1</sup>, أنوار حسن الصالح<sup>2</sup>, حيدر جواد محمد<sup>3\*</sup>, هبة خضير عباس<sup>4</sup>, علي عبد داود الزكي<sup>3</sup>

<sup>1</sup>قسم الحاسوب، كلية التربية الأساسية، الجامعة المستنصرية، بغداد، العراق

<sup>2</sup>قسم علوم الحاسوب، كلية العلوم، الجامعة المستنصرية، بغداد، العراق

<sup>3</sup>قسم الفيزياء، كلية العلوم، الجامعة المستنصرية، بغداد، العراق

<sup>4</sup>قسم الفيزياء، كلية العلوم للبنات، جامعة بغداد، بغداد، العراق

### الخلاصة

يؤدي تحليل نسيج الخلايا السرطانية إلى إجراء لتمييز الاختلافات المكانية داخل الصورة واستخراج المعلومات المهمة. تُستخدم صورتان اختباريتان مع الأورام لتحديد نوع السرطان وموقعه وخصائصه الهندسية

\*Email: [Rashaheart\\_2005@uomustansiriyah.edu.iq](mailto:Rashaheart_2005@uomustansiriyah.edu.iq)

(المنطقة والحجم والأبعاد ونصف القطر وما إلى ذلك) في هذه الدراسة. تم تصميم الخوارزمية المقترحة لاكتشاف وتمييز سرطان الثدي باستخدام تقنية العتبة القائمة على التجزئة. طريقة تحليل النسيج تم استخدام طريقة منطقة حجم المستوى الرمادي لاستخراج 11 ميزة: التركيز على المنطقة الصغيرة ، التركيز على المنطقة الكبيرة ، التركيز على المستوى الرمادي المنخفض ، التركيز على المنطقة الرمادية العالية ، التركيز على المستوى الرمادي المنخفض للمنطقة الصغيرة ، التركيز على المستوى الرمادي المنخفض للمنطقة الصغيرة ، التركيز على المستوى الرمادي المرتفع للمنطقة الكبيرة ، المستوى الرمادي غير التوحيد الطبيعي ، المستوى الرمادي عدم التوحيد ، والنسبة المئوية للمنطقة. أظهرت النتائج أن مكان الورم يتميز بدقة عالية حسب خصائص الاستخلاص. نتائج الطريقة المقترحة تعطي القرار لتحديد نوع الأورام. تساعد هندسة الورم في وصف الورم.

## 1. Introduction

Breast cancer is the most public disease among women worldwide [1-3]. As a method of human imaging tissue, magnetic resonance imaging (MRI) is increasingly used in private clinics and for research purposes to diagnose breast cancer [4-6]. The change in tumour size requests a routine MRI test to address the response of the treatment by a specialist [7, 8]. The check needs to have the tumour details like position, dimensions, and radius to be compared with the new test [9]. The breast tumour has two types: malignant and benign [10, 11]; the malignant type is grown rapidly and fed from blood cells. In contrast, benign tumours grow slower and consider not harmful to human health [12].

One of the analyzing texture feature methods is the characterization of histogram intensity, but it refers to spatial and frequency details [13]. Several studies presented radiomics analysis for breast tumour classification and detection based on texture features [14, 15], leading to a study of contrast-enhanced mammography with a range of specificity of 58-70% [16]. The automatic characterization algorithms address the features within the studied images to represent the biological data for tumour and related diseases [17]. Consequent analysis, statistics, classification, and nomogram describe image features in the image [18]. Some studies of MRI to diagnose breast cancer are based on radiomics quantified analysis [19].

There were attempts to evaluate several features of breast parenchyma, but it requires profound analysis [20-22]. In 2014, Marina Milosevic *et al.* used feature-based extraction and image segmentation techniques to detect and diagnose abnormal patterns in thermal breast charts. Vector Machine support class, the Naive Bayes classifier, and the K-Nearest Neighbour class are used to distinguish abnormally from normal tissue with an accuracy of 92.5% [23]. In 2019, Abiwinanda *et al.* introduced a method for digital mammogram classification features depending on the Shearlet transform. They used the transform over the image to build the feature vectors using the transform's coefficients. T-test statistics calculation is used to rank the features and distinguish between classes. They must use the threshold step to represent better classes and support vector machine (SVM) classifiers [24].

In this study, mammography images (breast tumours) have been studied to extract features of normal and cancer regions. The geometric properties are extracted using Grey Level Size Zone Matrix, Classification Texture chromatically, and segmentation algorithms. The tumour regions are extracted precisely with valuable high-level information to the specialist.

## 2. Material and Methods

The analysis and classification of image texture are the first steps to isolating the tumour region [25]. The test images with two types of tumours are presented in Figure 1.

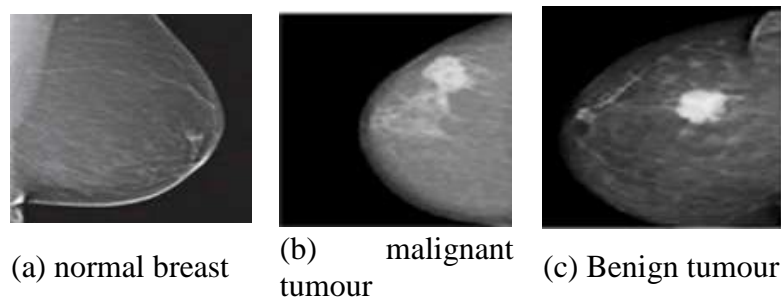


**Figure 1:** The mammography breast images for (a) normal, (b) malignant, and (c) benign. The diagram chart in Figure 2 includes steps showing the detection, separation, detection of healthy and non-healthy regions, and calculating geometric properties.

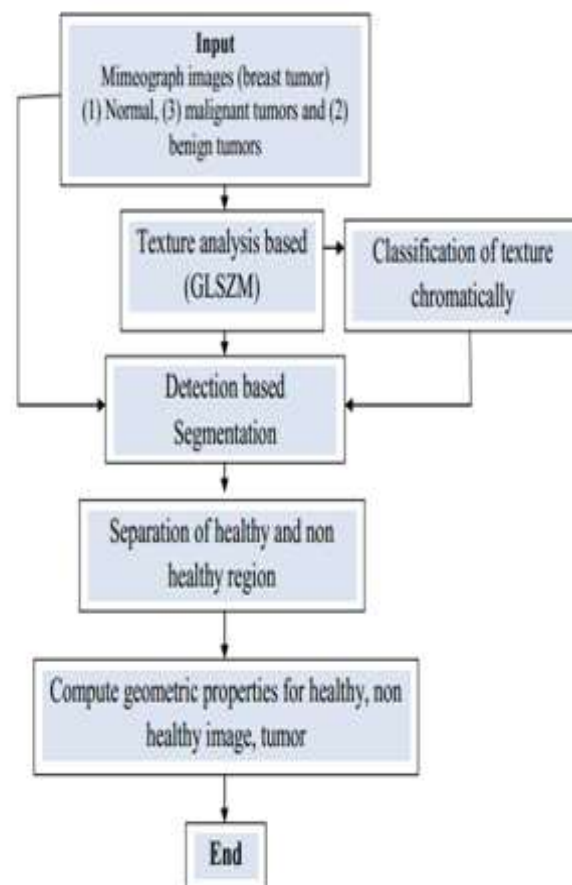


**Figure 2:** Suggested diagram to extract the geometric features.

### 2.1 Grey Level Size Zone Matrix (GLSZM)

The grey level size zone matrix (GLSZM) was used because it sums up the data of similar groups of connected voxels with specific discredited pixels values and sizes [26]. These voxels are linked if the surrounding voxels have the same pixel values. In the 3-D view of texture analysis, there are 26-connectedness considered to represent any of the similar 26 adjacent voxels with the equal grey level of the center voxel. In the 2-D view, there are 8-connectedness used. An issue with 2-D approaches is that voxels are connected across slices but disconnected within the slice plane.

The total number of zones can be written as:

$$N_s = \sum_{i=1}^{N_g} \sum_{j=1}^{N_z} S_{ij} \tag{1}$$

where  $S$  is the zone number with discredited grey level  $i$  with  $j$  and can represent  $N_g \times N_z$  grey level.  $N_g$  has discredited grey levels, and  $N_z$  is the maximum zone size of a group, or zone, of connected voxels with the same grey level value. Marginal sums can be presented as:

$$S_i = \sum_{j=1}^{N_z} S_{ij} \tag{2}$$

where  $S_i$  is the zone number with discredited grey level  $i$ . Similarly, the number of zones with size  $j$  can be written as:

$$S_j = \sum_{i=1}^{N_g} S_{ij} \tag{3}$$

Figure 3 shows an example of a matrix calculation of an image to express the method idea.

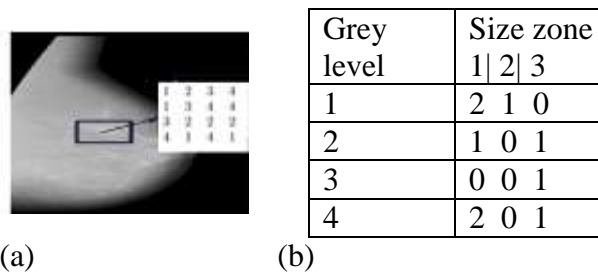


**Figure 3:** GLSZM filling example for (a) a  $4 \times 4$  image texture dimensions (b) 4 grey levels and using 8-connectivity [27].

The texture zone direction represents the size zone matrices listed in Table 1; the given size zone is represented by  $S(i, j)$ .

**Table 1:** The studied features with its equation for the GLSZM [18]

Texture GLSZM Features	Relation
Small Zone Emphasis (SZE)	$F_{SZE} = \frac{1}{N_s} \sum_{j=1}^{N_z} \frac{S_j}{j^2}$
Large Zone Emphasis(LZE)	$F_{LZE} = \frac{1}{N_s} \sum_{j=1}^{N_z} j \cdot S_j$
Low Grey Level Zone Emphasis (LGZE)	$F_{LGZE} = \frac{1}{N_s} \sum_{i=1}^{N_g} \frac{S_i}{i^2}$
High Grey Level Zone Emphasis (HGZE)	$F_{HGZE} = \frac{1}{N_s} \sum_{i=1}^{N_g} i \cdot S_i$
Small Zone Low Grey Level Emphasis(SZLGE)	$F_{SZLGE} = \frac{1}{N_s} \sum_{i=1}^{N_g} \sum_{j=1}^{N_z} \frac{S_{ij}}{i^2 j^2}$
Small Zone High Grey Level Emphasis(SZHGE)	$F_{SZHGE} = \frac{1}{N_s} \sum_{i=1}^{N_g} \sum_{j=1}^{N_z} \frac{i^2 S_{ij}}{j^2}$
Large Zone Low Grey Level Emphasis(LZLGE)	$F_{LZLGE} = \frac{1}{N_s} \sum_{i=1}^{N_g} \sum_{j=1}^{N_z} \frac{j^2 S_{ij}}{i^2}$

Large Zone High Grey Level Emphasis(LZHGE)	$F_{LZHHE} = \frac{1}{N_S} \sum_{i=1}^{N_g} \sum_{j=1}^{N_z} i^2 j^2 S_{ij}$
Grey Level Non-Uniformity Normalised (GLNUN)	$F_{GLNUN} = \frac{1}{N_S} \sum_{i=1}^{N_g} S_i^2$
Grey Level Non-Uniformity (GLNU)	$F_{GLNU} = \frac{1}{N_S^2} \sum_{i=1}^{N_g} S_i^2$
Zone Percentage(ZP)	$F_{ZP} = \frac{N_S}{N_V}$

### 2.1.1 Algorithms GLSZM

Input: breast image (img) with all types.

Output: feature image (imgFR) which are 11 features.

Start algorithm

Step1: load img

Step2: use `imgy=rgb2gray(img)` to convert image.

Step3: run windows (5×5), `A= img(m:m+4,n:n+4,)` m :number of row, n: number of column

Step4: find function code in MATLAB used to find the size zone. It is applied for all pixel value in (A), `A1=A==1; s1 = region props(A1); a1=[s1.Area]; L1=length(a1);`

Step5: calculate each gray level in all directions and according to the size zone as:

for `i=1:L1`

`t=a1(i);`

`B(1,t)=B(1,t)+1;`

end

where *i* grey level and *t* size zone for grey level; B: size zone image for all image pixel value.

Step6: find normalized size zone value: image (Bn)

•find `B = B'` to get `Bcount = B+B'`.

•find  $\Sigma$  of `Bcount = H`

•find `Bn=Bcount/H`

Step 7: find Bn to calculate size zone features (imgFS)

End algorithm

### 2.1.2 Classification Texture chromatically algorithm

Input: load (imgy), (imgFS)

Output: Image classified chromatically(imgC)

Start algorithm

Step1: get img

Step2: use `imgy=rgb2gray(img)code` to transfer img to gray image

Step3: Divide the image into 5 grayscale levels: `img2=round (img (5/255));`

Step4: `imgC= zero(r,c,3)` where *r* number of row, *c* number of column

if `img2(i,j)==1`

`B(i,j,:)= [255 0 0];`

else if `img2(i,j)==2`

`B(i,j,:)= [0 255 0];`

else if `img2(i,j)==3`

`B(i,j,:)= [0 0 255];`

else if `img2(i,j)==4`

`B(i,j,:)= [90 100 200];`

else if `img2(i,j)==5`

```

    B(i,j,:)= [200 100 60];
    end; end; end; end; end;
Step6: convert imgC using uint8, then save (imgC)
End algorithm

```

## 2.2 Segmentation-Based Threshold

In segmentation methods, an image is divided into several small segments, where the goal is to identify the correct areas and analyze the diagnosis [28]. In this study, the segmentation-based threshold technique of early and accurate breast tumors detection is used for diagnosis and continuous follow-up of treatment of patients before their progression to patients with tumours. The segmented image is implemented on a binary image with a specially selected threshold through which the image is fragmented. The suggested algorithm used to segment medical images is shown in the following algorithm, and the results are shown in figure 4.

### 2.2.1 Segmentation Algorithm

Input: load (imgy) and (imgFS)

Output: Tumour (T) and complement (C) image and histogram of tumour (hist T) and complement (hist C) for each (img) and each (imgFS).

Start algorithm

Step1: load imgy and imgFS and display

Step2: convert imgy to binary image (imgB) for code  $imgB = im2bw(imgy, th)$ ; where  $th$  is threshold

Step3: display image  $imgB = imO$  then apply morphological process (clean and fill), where clean = remove isolated pixel, fill = fill isolated interior pixels.

Step4: Find object area [MAX A imx ], and its location accurately idx

Step 5: Calculate the area for imgB and img C for each imgy and imgF

Step6: plot histogram of tumour feature image  $(TF) = (imgFS.) \times (imO)$

Step7: plot  $(imgC) = T - imgy$  or  $img(imgCF) = TF - imgF$  with histogram

End algorithm

## 3. Results and Discussion

For clarity, normal breast image results are not shown due to no essential details. Therefore, the remaining images are studied intensively. Figure 5 shows the shape and location of the tumour in the image, which appeared when the 11 features were applied. These features are helpful to distinguish the tumour details and reach an excellent level of isolation. Figures 6 and 7 presented the results of applying the suggested algorithms using malignant and benign images; all features are presented clearly and show the difference in details between the original, tumor, and complement images. They were also giving more information, like showing the histogram of each feature for all images. This indicates the details of the tumour or the objects within the image.

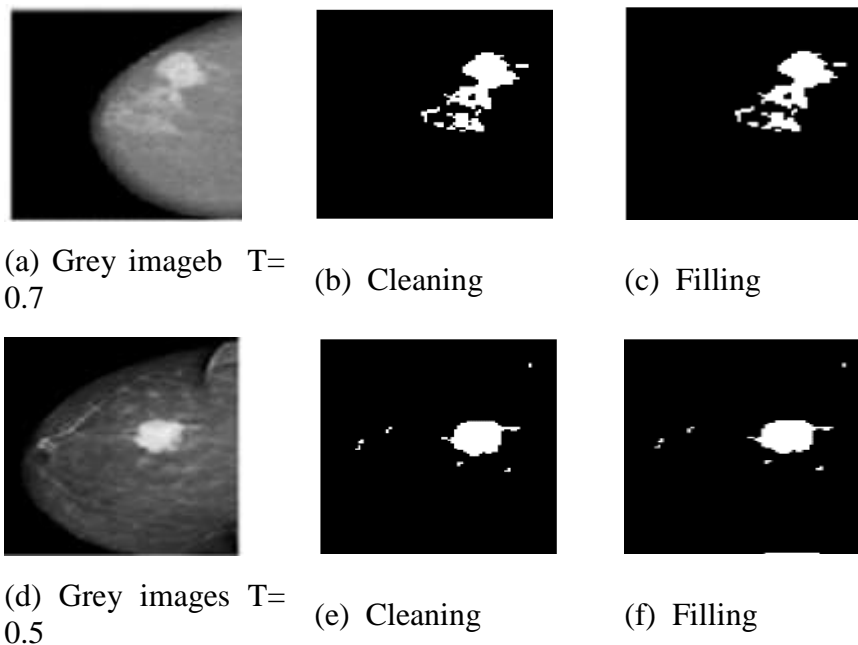
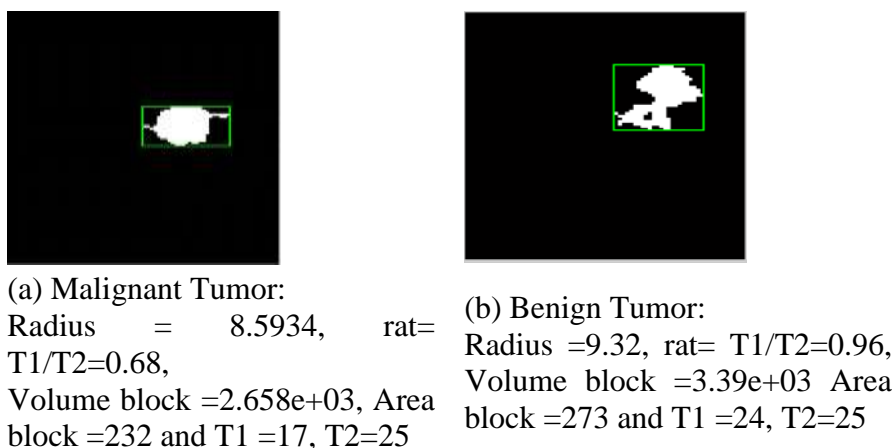


**Figure 4:** (a and d) Grey images using threshold value and (b, c, e, and f) the morphological techniques (Filling and cleaning)



(a) Malignant Tumor:  
 Radius = 8.5934, rat=  
 $T1/T2=0.68$ ,  
 Volume block =2.658e+03, Area  
 block =232 and  $T1 =17$ ,  $T2=25$

(b) Benign Tumor:  
 Radius =9.32, rat=  $T1/T2=0.96$ ,  
 Volume block =3.39e+03 Area  
 block =273 and  $T1 =24$ ,  $T2=25$

**Figure 5:** The concluded data of the tumour studied images using proposed algorithms.

The shape of the green box shows the tumor type and confirms our idea of distinguishing between Malignant and Benign tumors. The area of the tumour does not depend on the green box size but the white pixels. It is essential to notice the parameters  $T1$  and  $T2$ , representing the green box's height and width. These parameters indicate tumour type, and it is the first time to present new parameters to interpret image details.

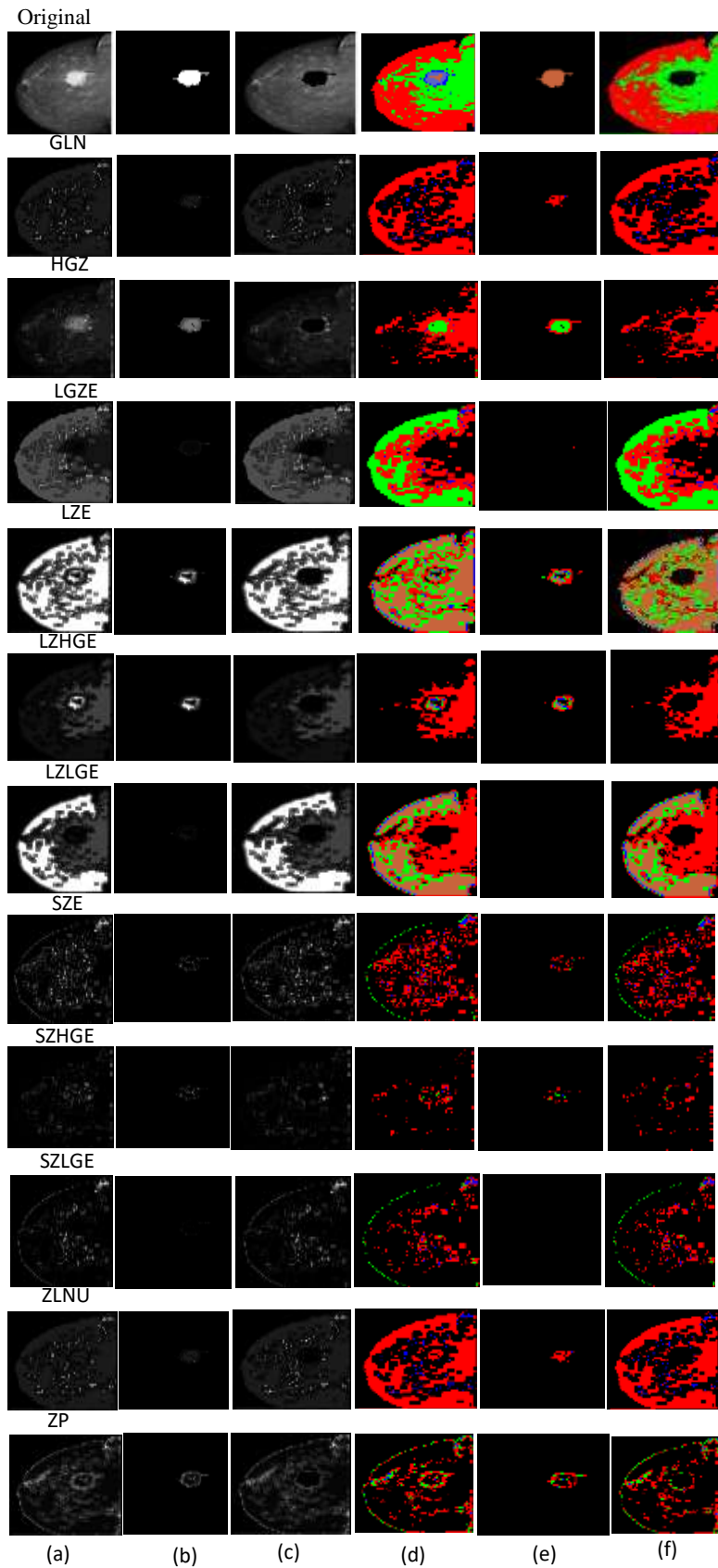


**Figure 7:** The benign image (a) studied image with 11 features (b) Tumour image, (c) complement image, (d, e, f) The malignant image, tumour, and complement images after classified texture chromatically



### 3.1 Statistical output for malignant and benign images

Figure 8 shows the statistical results of the origin, malignant, and benign images. These results are essential to show the differences among all types of images. Moreover, the feature behavior is evident in this case and can distinguish each feature's property. In conclusion, we refer to these results and clarify each feature's strong and weak points. It is essential to notice that the y-axis scale with malignant data in Figure 8 (b) is 7000 (a.u.) while benign data for the same scale in Figure 8 (e) is 8000 (a.u.). The behavior is different and can be noticed from the statistical data.

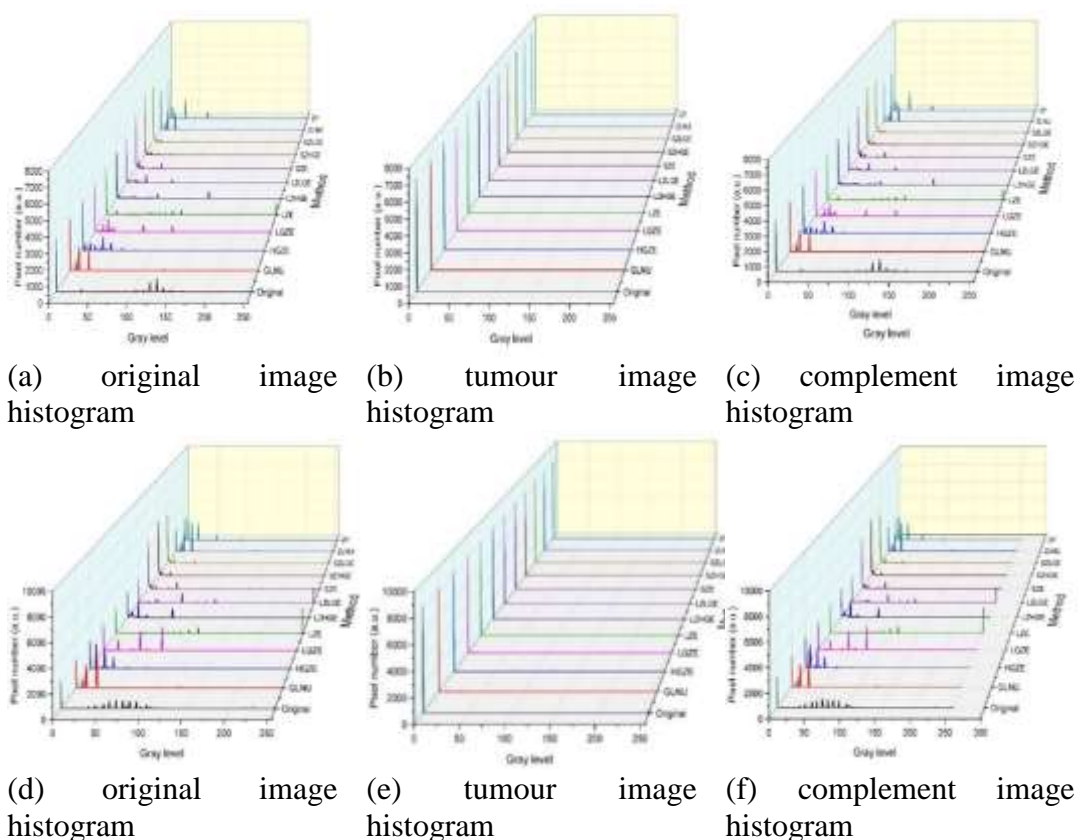


**Figure 8:** The histogram of feature for malignant image (a) original image, (b) tumour image, (c) complement image, and histogram of feature for benign image (d) original image, (e) tumour image, and (f) complement image.

### 4. Conclusion

The tumour histogram or supplementary image shows the behavior of the tissue trait for each image. The type of tumour can be known from the dimensions as new parameters are presented. If T1 and T2 approximately have the same value, then the tumour is benign; else, the tumour is malignant. The output of the proposed GLSZM method showed more details and is terminologically accurate than the histogram's pixel points (compared with the original image). The output value is null for the same region in the original image—the GLSZM output relay on the grey level value.

The behavior of some features is changed with tumour segregation in the histogram results; for instance, SZE and SZHGE have SZLGE ruling in malignant and benign tumours. With the complementary image and comparing the results with other researchers, the methods of SGLCM, GLRLM, and GLCM with the proposed method (GLSZM) are similar in output

data, except that the GLRLM method and SGLCM were more accurate in separating tumours. The histogram results are evident and accurate in identifying and extracting the tumour area. Accuracy depends on tumour and supplementary image histogram. This method shows the shifting in the contribution of the pixel value within the tumour; the supplementary image is evident.

## References

- [1] W. Ayele *et al.*, "Breast cancer morbidity and mortality in rural Ethiopia: data from 788 verbal autopsies," *BMC Women's Health*, vol. 22, no. 1, p. 89, 2022/03/24 2022, doi: 10.1186/s12905-022-01672-7.
- [2] Q. Peng and X. Ren, "Mapping of Female Breast Cancer Incidence and Mortality Rates to Socioeconomic Factors Cohort: Path Diagram Analysis," (in English), *Frontiers in Public Health*, Original Research vol. 9, 2022-February-01 2022, doi: 10.3389/fpubh.2021.761023.
- [3] F. N. C. Leitão *et al.*, "Breast and cervical cancer mortality in the western Amazon: A time series study between 1980 and 2014," (in eng), *Medicine (Baltimore)*, vol. 100, no. 21, pp. e26157-e26157, 2021, doi: 10.1097/MD.00000000000026157.
- [4] S. Sharma, F. G. Vicenty-Latorre, S. Elsherif, and S. Sharma, "Role of MRI in Breast Cancer Staging: A Case-Based Review," (in eng), *Cureus*, vol. 13, no. 12, pp. e20752-e20752, 2021, doi: 10.7759/cureus.20752.
- [5] Y.-M. Lei *et al.*, "Artificial Intelligence in Medical Imaging of the Breast," (in eng), *Front Oncol*, vol. 11, pp. 600557-600557, 2021, doi: 10.3389/fonc.2021.600557.
- [6] A. Iqbal and M. Sharif, "MDA-Net: Multiscale dual attention-based network for breast lesion segmentation using ultrasound images," *Journal of King Saud University - Computer and Information Sciences*, 2021/10/21/ 2021, doi: <https://doi.org/10.1016/j.jksuci.2021.10.002>.
- [7] A. Sobhi, S. Talaat hamed, E.-s. Hussein, S. Lasheen, M. Hussein, and Y. Ebrahim, "Predicting pathological response of locally advanced breast cancer to neoadjuvant chemotherapy: comparing the performance of whole body 18F-FDG PETCT versus DCE-MRI of the breast," *Egyptian Journal of Radiology and Nuclear Medicine*, vol. 53, no. 1, p. 79, 2022/03/31 2022, doi: 10.1186/s43055-022-00743-x.
- [8] D. Lau *et al.*, "Multiparametric MRI of early tumor response to immune checkpoint blockade in metastatic melanoma," (in eng), *J Immunother Cancer*, vol. 9, no. 9, p. e003125, 2021, doi: 10.1136/jitc-2021-003125.
- [9] O. M. Henriksen *et al.*, "High-Grade Glioma Treatment Response Monitoring Biomarkers: A Position Statement on the Evidence Supporting the Use of Advanced MRI Techniques in the Clinic, and the Latest Bench-to-Bedside Developments. Part 1: Perfusion and Diffusion Techniques," (in English), *Front Oncol*, Review vol. 12, 2022-March-03 2022, doi: 10.3389/fonc.2022.810263.
- [10] W. Al Noumah, A. Jafar, and K. Al Joumaa, "Using parallel pre-trained types of DCNN model to predict breast cancer with color normalization," *BMC Research Notes*, vol. 15, no. 1, p. 14, 2022/01/10 2022, doi: 10.1186/s13104-021-05902-3.
- [11] G. Ayana, J. Park, and S.-w. Choe, "Patchless Multi-Stage Transfer Learning for Improved Mammographic Breast Mass Classification," *Cancers*, vol. 14, no. 5, 2022, doi: 10.3390/cancers14051280.
- [12] S. Aklilu *et al.*, "Evaluation of diagnostic ultrasound use in a breast cancer detection strategy in Northern Peru," *PLOS ONE*, vol. 16, no. 6, p. e0252902, 2021, doi: 10.1371/journal.pone.0252902.
- [13] F. Bianconi, A. Fernández, F. Smeraldi, and G. Pascoletti, "Colour and Texture Descriptors for Visual Recognition: A Historical Overview," *Journal of Imaging*, vol. 7, no. 11, 2021, doi: 10.3390/jimaging7110245.
- [14] S. Hasan, A. Sagheer, and H. Veisi, "Breast Cancer Classification Using Machine Learning Techniques: A Review," *Turkish Journal of Computer and Mathematics Education (TURCOMAT)*, vol. 12, pp. 1970-1979, 09/18 2021.
- [15] R. Shubair, *Comparative Study of Machine Learning Algorithms for Breast Cancer Detection and Diagnosis*. 2016.

- [16] S. Muhtadi, "Breast Tumor Classification Using Intratumoral Quantitative Ultrasound Descriptors," *Computational and Mathematical Methods in Medicine*, vol. 2022, p. 1633858, 2022/03/07 2022, doi: 10.1155/2022/1633858.
- [17] H. K. Abbas, A. H. Mahdy, A. A. Al Zuky, and S. F. Ahmad, "Analytical Study of Medical Image Combination Techniques," *Iraqi Journal of Science*, vol. 59, no. 3B, pp. 1538-1547, 08/30 2018. [Online]. Available: <https://ijs.uobaghdad.edu.iq/index.php/eijs/article/view/429>.
- [18] A. S. Derea, H. K. Abbas, H. J. Mohamad, and A. A. Al-Zuky, "Adopting Run Length Features to Detect and Recognize Brain Tumor in Magnetic Resonance Images," in *2019 First International Conference of Computer and Applied Sciences (CAS)*, 18-19 Dec. 2019 2019, pp. 186-192, doi: 10.1109/CAS47993.2019.9075718.
- [19] S. Niu *et al.*, "Radiomic Evaluations of the Diagnostic Performance of DM, DBT, DCE MRI, DWI, and Their Combination for the Diagnosis of Breast Cancer," (in English), *Front Oncol*, Original Research vol. 11, 2021-September-10 2021, doi: 10.3389/fonc.2021.725922.
- [20] A. Gastounioti, E. F. Conant, and D. Kontos, "Beyond breast density: a review on the advancing role of parenchymal texture analysis in breast cancer risk assessment," *Breast Cancer Research*, vol. 18, no. 1, p. 91, 2016/09/20 2016, doi: 10.1186/s13058-016-0755-8.
- [21] A. A. Mohamed, W. A. Berg, H. Peng, Y. Luo, R. C. Jankowitz, and S. Wu, "A deep learning method for classifying mammographic breast density categories," (in eng), *Med Phys*, vol. 45, no. 1, pp. 314-321, 2018, doi: 10.1002/mp.12683.
- [22] K. Shaffer, "Mammographic Parenchymal Analysis: Can We Do Better with Digital Assistance?," *Radiology*, vol. 291, no. 1, pp. 21-22, 2019/04/01 2019, doi: 10.1148/radiol.2019190085.
- [23] M. Milosevic, D. Jankovic, and A. Peulic, "Thermography based breast cancer detection using texture features and minimum variance quantization," (in eng), *EXCLI J*, vol. 13, pp. 1204-1215, 2014. [Online]. Available: <https://pubmed.ncbi.nlm.nih.gov/26417334>.
- [24] N. Abiwinanda;, M. Hanif;, S. T. Hesaputra;, A. Handayani;, and T. R. Mengko, "Brain Tumor Classification Using Convolutional Neural Network," in *World Congress on Medical Physics and Biomedical Engineering 2018*: Springer Singapore, 2019, pp. 183-189.
- [25] M. Khened, A. Kori, H. Rajkumar, G. Krishnamurthi, and B. Srinivasan, "A generalized deep learning framework for whole-slide image segmentation and analysis," (in eng), *Sci Rep*, vol. 11, no. 1, pp. 11579-11579, 2021, doi: 10.1038/s41598-021-90444-8.
- [26] H. K. Abbas, N. A. Fatah, H. J. Mohamad, and A. A. Alzuky, "Brain Tumor Classification Using Texture Feature Extraction," *Journal of Physics: Conference Series*, vol. 1892, 2021.
- [27] G. Thibault *et al.*, "Texture indexes and gray level size zone matrix. Application to cell nuclei classification," 2009.
- [28] E. Michael, H. Ma, H. Li, F. Kulwa, and J. Li, "Breast Cancer Segmentation Methods: Current Status and Future Potentials," *BioMed Research International*, vol. 2021, p. 9962109, 2021/07/22 2021, doi: 10.1155/2021/9962109.